

Boosted Kerr black hole

Janusz Karkowski

4th May 2021

Institute of Physics, Jagellonian University, Reymonta 4, 30-059 Kraków,
Poland

Abstract

Initial data for boosted Kerr black hole are constructed in an axially symmetric case. Momentum and hamiltonian constraints are solved numerically using finite element method (FEM) algorithms. Both Bowen-York and puncture boundary conditions are adopted and appropriate results are compared. Past and future apparent horizons are also found numerically and the Penrose inequality is tested in detail.

PACS numbers: 04.20.Cr, 04.20.Dw, 04.70.Bw

1 Introduction

We will construct initial data for single boosted Kerr black hole in the axially symmetric case with the total momentum parallel to the angular momentum of the black hole. We assume also asymptotical flatness. Two popular approaches to the constructions of black hole initial data will be adopted. The first is the Bowen-York solution [1] based on the conformal transverse-traceless decomposition [3] of Einstein equations with certain additional assumptions such as conformal flatness and maximal slicing. The second is the puncture approach [2] developed by Brandt and Brügmann. Their idea was to remove analytically the coordinate singularity at the location of the black hole. In this way they avoided inner boundary conditions present in the Bowen-York approach. We follow these ideas as close as possible but some important modifications are necessary. Garat and Price [5] have proved nonexistence of conformally flat slices of the Kerr spacetime. Thus the assumption of conformal flatness must be abandoned. We assume maximal slicing in order to simplify the problem but in general it is not necessary. Our approach is straightforward. We use the quasi-isotropic radial coordinate [3], [4] in which it is easy to show that the Kerr solution is composed of two isometric regions smoothly joined at a sphere of some radius. Then the original Bowen-York inner boundary conditions can be applied. The momentum constraints in the axially symmetric case can be solved

analytically for the flat background metric [25], [20], and they can be solved numerically in the case of metrics which are not conformally flat. We solve the hamiltonian constraint using the finite element method (FEM) [8] techniques, then we find the apparent horizon and test the Penrose inequality.

Our paper consists of three parts. In the first we shortly review Einstein constraint equations. The second section discusses the numerical approach and special assumptions that are made there. The third part deals with detailed results.

2 Einstein Constraint Equations

2.1 ADM framework

In the Cauchy formulation of Einstein equations [9],[3] the whole 4-dimensional manifold is foliated into a set of the so-called slices. These slices are the 3-dimensional, spacelike surfaces labeled by a parameter t (time). The Einstein equations are projected onto these hypersurfaces. One obtains six evolution equations and four constraint equations that the metric, γ_{ij} , and the extrinsic curvature, K_{ij} , of each slice must satisfy. In the ADM (3+1) decomposition of the spacetime the metric can be written as

$$ds^2 = -N^2 dt^2 + \gamma_{ij}(dx^i + \beta^i dt)(dx^j + \beta^j dt). \quad (1)$$

The proper time between slices is given by the lapse function N and the coordinate drift between slices is described by the shift vector β^i . The evolution equations in a vacuum have the following form

$$(\partial_t - L_\beta)\gamma_{ij} = -2NK_{ij}, \quad (2)$$

$$(\partial_t - L_\beta)K_{ij} = (-\nabla_i \nabla_j + R_{ij} + KK_{ij} - 2K_{ik}K_j^k)N. \quad (3)$$

Here R_{ij} is the Ricci tensor on the slice, K is the trace of the extrinsic curvature and the covariant derivative ∇_i is taken with respect to the spatial metric γ_{ij} . L_β denotes the Lie derivative along the shift vector β^i .

The minimal set of initial data consisting of the 3-dimensional metric γ_{ij} and the extrinsic curvature K_{ij} cannot be specified independently on the initial slice. These data are constrained by four equations, as mentioned above, because the slices must fit properly into the 4-dimensional manifold. The first of these equations is known as the hamiltonian (or scalar) constraint

$$R + K^2 - K_{ij}K^{ij} = 0, \quad (4)$$

and the other three, called momentum (or vector) constraints read as

$$\nabla_j(K^{ij} - \gamma^{ij}K^l_l) = 0. \quad (5)$$

Here R denotes the Ricci scalar. Let us note that if the above constraint equations are satisfied on one initial hypersurface, the same holds true on each slice. It is also important that the constraint equations do not depend on the lapse function N and the shift vector β^i which can be freely chosen on each slice. This is the base of the (general) gauge invariance of the theory.

2.2 York-Lichnerowicz conformal approach

The process of solving of the constraint equations can be significantly simplified by the conformal York-Lichnerowicz decomposition [3], [1]:

$$\gamma_{ij} = \psi^4 \hat{\gamma}_{ij}, \quad (6)$$

$$K_{ij} = \hat{K}_{ij} \psi^{-2}. \quad (7)$$

The new metric $\hat{\gamma}_{ij}$ is called the conformal (or background) metric and can be chosen arbitrarily. This conformal transformation preserves the shape of the momentum constraints:

$$\hat{\nabla}_j (\hat{K}^{ij} - \hat{\gamma}^{ij} \hat{K}^l_l) = 0, \quad (8)$$

and the hamiltonian constraint can be rewritten as

$$\hat{\nabla}^2 \psi = \frac{1}{8} \hat{R} \psi - \frac{1}{8} (\hat{K}_{ij} \hat{K}^{ij} - (\hat{K}_i^i)^2) \psi^{-7}. \quad (9)$$

The covariant derivative $\hat{\nabla}$ and the Ricci scalar \hat{R} correspond to the background metric $\hat{\gamma}_{ij}$. We will also impose the maximal slicing condition

$$K = K_i^i = 0. \quad (10)$$

This equality can be understood as a gauge fixing condition. It fixes the lapse function N and is convenient in avoiding coordinate singularities during the time evolution of the system. It also simplifies the constraint equations which finally take the form

$$\hat{\nabla}_j \hat{K}^{ij} = 0, \quad (11)$$

$$\hat{\nabla}^2 \psi = \frac{1}{8} \hat{R} \psi - \frac{1}{8} \hat{K}_{ij} \hat{K}^{ij} \psi^{-7}. \quad (12)$$

2.3 Axially symmetric ansatz

We would like to solve numerically the constraint equations for the boosted Kerr black hole with momentum directed along angular momentum. Therefore it is desirable to choose a Weyl metric as the background metric. The Weyl metric is axially symmetric and its line element in the spherical coordinates has the form [10], [11]

$$\hat{\gamma}_{ij} dx^i dx^j = \exp(-q(r, \theta))(dr^2 + r^2 d\theta^2) + r^2 \sin^2 \theta d\phi^2. \quad (13)$$

Let us recall that the Kerr initial data can be written (in terms of quasi-isotropic radial coordinate r) as [3]

$$\exp(-q(r, \theta)) = \frac{\Sigma^2}{(R^2 + a^2)^2 - \Delta a^2 \sin^2 \theta}, \quad (14)$$

$$\Sigma = R^2 + a^2 \cos^2 \theta, \quad (15)$$

$$\Delta = R^2 - 2mR + a^2, \quad (16)$$

$$R = r + m + \frac{b^2}{r}, \quad (17)$$

$$b = \frac{\sqrt{m^2 - a^2}}{2}, \quad (18)$$

where m, a are Kerr parameters and the conformal factor $\psi(t, \theta)$ is given by

$$\psi^4(r, \theta) = \frac{\Sigma}{r^2} \exp(q(r, \theta)). \quad (19)$$

We will fix the $\exp(-q(r, \theta))$ factor in (13) to be that from the Kerr metric (14). The external curvature in the axially symmetric case with maximal slicing can be written in the form

$$(\hat{K}_{ij}) = \begin{pmatrix} \frac{f_{11}(r, \theta)}{r^2} & \frac{f_{12}(r, \theta) \sin \theta}{r} & \frac{f_{13}(r, \theta)}{r^2 \sin \theta} \\ \dots & f_{22}(r, \theta) & \frac{f_{23}(r, \theta)}{\sin \theta} \\ \dots & \dots & -\frac{(f_{11}(r, \theta) + f_{22}(r, \theta)) \sin^2 \theta}{\exp(-q(r, \theta))} \end{pmatrix}, \quad (20)$$

where $i, j = r, \theta, \phi$ and $\hat{K}_{ij} = \hat{K}_{ji}$. The momentum constraint equations (11) reduce then to

$$r \partial_r(r f_{11}) + \frac{1}{2} r^2 (f_{11} + f_{22}) \partial_r q - \partial_y((1 - y^2) r f_{22}) = 0, \quad (21)$$

$$\partial_r((1 - y^2) r f_{12}) - \frac{1 - y^2}{2} (f_{11} + f_{22}) \partial_y q - \partial_y((1 - y^2) f_{22}) + y f_{11} = 0, \quad (22)$$

$$\partial_r f_{13} + \partial_\theta f_{23} = 0. \quad (23)$$

The axial symmetry allows one to solve these equations by the method of separating variables. The functions f_{13} and f_{23} are present in the third equation only. This equation can be easily integrated. The result is

$$f_{13} = -\partial_\theta Z(r, \theta), \quad (24)$$

$$f_{23} = \partial_r Z(r, \theta), \quad (25)$$

where $Z(r, \theta)$ is an arbitrary function. If we put

$$f_{11} = f_{12} = f_{22} = 0, \quad (26)$$

$$Z(r, \theta) = ma(\cos^3 \theta - 3 \cos \theta) - \frac{ma^3 \sin^4 \theta \cos(\theta)}{\Sigma}, \quad (27)$$

then we recover the full Kerr initial data.

3 Numerical approach

3.1 Momentum constraints

The background metric becomes flat for $q(r, \theta) = 0$. This is the case when the angular momentum of the Kerr black hole is equal to zero and we get the Schwarzschild solution. Thus for $a = 0$ we have the flat background metric and then the momentum constraints can be solved analytically (assuming maximal slicing and axial symmetry). The solution reads as [6]

$$\hat{K}_{rr} = \frac{1}{r^3} \partial_y^2 W(r, \theta), \quad (28)$$

$$\hat{K}_{r\theta} = \frac{1}{r \sin \theta} \partial_y \partial_r W(r, \theta), \quad (29)$$

$$\hat{K}_{\theta\theta} = \frac{1}{\sin^2 \theta} (\partial_r (r \partial_r W(t, \theta)) + \frac{1}{r} (y \partial_y W(r, \theta) - W(r, \theta))), \quad (30)$$

$$\hat{K}_{r\phi} = \frac{1}{r^2} \partial_y Z(r, \theta), \quad (31)$$

$$\hat{K}_{\theta\phi} = \frac{1}{\sin \theta} \partial_r Z(r, \theta), \quad (32)$$

where $y = \cos \theta$ and W, Z are arbitrary functions. The component $\hat{K}_{\phi\phi}$ can be calculated from the maximal slicing condition $\hat{K}_i^i = 0$. These formulae can be obtained as a special case of Dain-Friedrich [7] conformally flat initial data that have been written in the Newman-Penrose formalism, or more simply by a direct integration of the momentum constraint equations (21-23).

Our idea is to obtain the momentum constraint solutions as a deformation of the above flat background formulae with a as the deformation parameter. Thus we look for solutions in the form

$$\hat{K}_{ij}(a) = \hat{K}_{ij}(a = 0) + \delta \hat{K}_{ij}(a). \quad (33)$$

where $\hat{K}_{ij}(a = 0)$ are given above and $\delta \hat{K}_{ij}(a)$ will be found numerically from (20),(21-22) with appropriate boundary conditions which will be discussed below.

3.2 Hamiltonian constraint

Numerical methods are necessary in order to solve the hamiltonian constraint in both flat and Weyl background metric. This constraint is a quasilinear elliptic equation and can be solved by the standard Newton method. The equation has the form

$$L\psi = F(r, \theta, \psi), \quad (34)$$

$$F(r, \theta, \psi) = f(r, \theta) \psi^{-7}, \quad (35)$$

where L is a linear operator and F, f are arbitrary functions. Let ψ_n be the n-th approximation in the Newton sequence. Then the following recurrence formula

can be easily obtained

$$(L - F_\psi(r, \theta, \psi_n))\delta\psi_n = F(r, \theta, \psi_n) - F(r, \theta, \psi_{n-1}), \\ -F_\psi(r, \theta, \psi_{n-1})(\psi_n - \psi_{n-1}).$$

Here $\delta\psi_n$ is a correction to the n -th approximation and F_ψ denotes the partial derivative of F with respect to ψ . It is important that the conformal factor ψ (19) is the analytical solution of (9) for Kerr initial data. Therefore it is an excellent example for testing of numerical methods and can serve as the 0-th order approximation to more complicated cases.

3.3 Bowen-York boundary conditions

Bowen and York demand the metric γ_{ij} and the external curvature K_{ij} to be invariant (up to a sign) under inversion through a sphere of radius b [1], [4]. This transformation is given in spherical coordinates by

$$\bar{r} = \frac{b^2}{r}, \bar{\theta} = \theta, \bar{\phi} = \phi. \quad (36)$$

The metric γ_{ij} is invariant if the background metric $\hat{\gamma}_{ij}$ is flat and if the conformal factor $\psi(r, \theta, \phi)$ satisfies

$$\psi(r, \theta, \phi) = \frac{b}{r}\psi(\bar{r}, \bar{\theta}, \bar{\phi}). \quad (37)$$

The same holds true for Weyl background metric (13) if the function $q(r, \theta)$ is invariant under the inversion transformation. This is the case for the Kerr metric with b given in (18). The invariance of the extrinsic curvature is equivalent to the following transformation rules

$$\begin{aligned} \hat{K}_{rr}(r, \theta, \phi) &= \pm \frac{b^6}{r^6} \hat{K}_{rr}(\bar{r}, \bar{\theta}, \bar{\phi}), \\ \hat{K}_{r\theta}(r, \theta, \phi) &= \mp \frac{b^4}{r^4} \hat{K}_{r\theta}(\bar{r}, \bar{\theta}, \bar{\phi}), \\ \hat{K}_{\theta\theta}(r, \theta, \phi) &= \pm \frac{b^2}{r^2} \hat{K}_{\theta\theta}(\bar{r}, \bar{\theta}, \bar{\phi}), \\ \hat{K}_{\theta\phi}(r, \theta, \phi) &= \mp \frac{b^2}{r^2} \hat{K}_{\theta\phi}(\bar{r}, \bar{\theta}, \bar{\phi}), \\ \hat{K}_{\phi\phi}(r, \theta, \phi) &= \pm \frac{b^2}{r^2} \hat{K}_{\phi\phi}(\bar{r}, \bar{\theta}, \bar{\phi}). \end{aligned} \quad (38)$$

We construct a family of invariant solutions of momentum constraints (11) for the flat background metric by putting the generating function $W(r, \theta)$ in formulae (28-30) equal to

$$\partial_y W(r, \theta) = -\frac{3}{2}P(r \pm \frac{b^2}{r}) \sin^2 \theta g(\theta), \quad (39)$$

where P is a parameter and $g(\theta)$ an arbitrary function. Let us note that for $g(\theta) = 1$ a Bowen-York solution is usually written in cartesian coordinates in

the form [1]

$$\hat{K}_{ij} = \frac{3}{2r^2} (P_i n_j + P_j n_i - (\eta_{ij} - n_i n_j) P^k n_k) \mp \frac{3b^2}{2r^4} (P_i n_j + P_j n_i - (\eta_{ij} - 5n_i n_j) P^k n_k), \quad (40)$$

where n_i is the unit normal to a sphere $r = \text{const}$. In this case P_i is the total linear momentum

$$P_i = \frac{1}{8\pi} \int K_{ij} d^2 S^j, \quad (41)$$

directed along z-axis. The appropriate formulae for the Weyl background metric result from (39) plus some corrections (which become zero for $a = 0$) that satisfy symmetry conditions (38). We get the following boundary conditions for corrections to the extrinsic curvature functions (22)

$$\begin{aligned} \partial_r \delta f_{11}(b, \theta) + \frac{1}{b} \delta f_{11}(b, \theta) &= 0, \\ \delta f_{12}(b, \theta) &= 0, \\ \lim_{r \rightarrow \infty} \delta f_{11}(r, \theta) &= \lim_{r \rightarrow \infty} \delta f_{12}(r, \theta) = 0. \end{aligned}$$

The function f_{22} can be chosen arbitrary. It is reasonable to keep the same relation between f_{11} and f_{22} as in the flat background case, that is

$$f_{11} + \frac{1}{2} f_{22} = 0.$$

The boundary conditions for the conformal factor ψ result from (37) (and asymptotical flatness) and read as

$$\begin{aligned} \partial_r \psi(b, \theta) + \frac{1}{2b} \psi(b, \theta) &= 0, \\ \lim_{r \rightarrow \infty} \psi(r, \theta) &= 1. \end{aligned}$$

3.4 Puncture boundary conditions

In the Bowen-York approach each slice consists of two isomorphic ends (the inversion transformation (36) defines an isometry of the physical metric) separated by a sphere of radius b and we can limit ourselves to one end without any singularities. The puncture method takes care of singularities in another way. In the flat background case we start with the curvature generated by

$$\partial_y W(r, \theta) = -\frac{3}{2} P r \sin^2 \theta g(\theta), \quad (42)$$

and continue with the conformal factor of the form

$$\psi = 1 + \frac{m}{2r} + \delta\psi, \quad (43)$$

where $\delta\psi$ is assumed to be nonsingular on the whole initial slice. Inserting (43) into (9) it can be easily seen that the admissible singularities (at $r = 0$) in

curvature functions are of type at most r^{-3} . That is why the term of order r^{-1} from (39) had to be excluded in (42).

The above formulae can be generalized to the Kerr background case in the following manner. The flat curvature functions are completed by (a -dependent) corrections in order to satisfy momentum constraint equations (22). These corrections are expected to be nonsingular. The form of the conformal factor (43) is changed to

$$\psi_{punc} = \psi + \delta\psi, \quad (44)$$

where ψ is given in (19). The correction $\delta\psi$ must also be nonsingular. This becomes clear if we compare (43) with the asymptotic expansions of ψ near $r = 0$ and $r = \infty$

$$\begin{aligned} \psi(r \approx 0, \theta) &= \frac{\sqrt{m^2 - a^2}}{2r} + \frac{m}{\sqrt{m^2 - a^2}} + \frac{a^2 r}{\sqrt{m^2 - a^2}^3} + O(r^2), \\ \psi(r \rightarrow \infty, \theta) &= 1 + \frac{m}{2r} + \frac{1}{8} \frac{a^2}{r^2} + O(\frac{1}{r^3}). \end{aligned}$$

Let us note that the boundary conditions for $r \rightarrow \infty$ are the same as in the Bowen-York case, for instance

$$\lim_{r \rightarrow \infty} \delta\psi(r, \theta) = 0.$$

4 Numerical results

4.1 Numerical techniques

The first step is to find the mapping of the radial coordinate onto some compact interval. In the Bowen-York case we have used a new coordinate x defined by

$$x = \frac{b}{r},$$

which maps the interval $[b, \infty)$ onto $[0, 1]$. Similarly, for puncture boundary conditions we have put

$$x = \frac{r}{1+r}.$$

In both cases we have to solve elliptic partial differential equations on the rectangle $[[0, 1], [-1, 1]]$ with mixed boundary conditions. These equations for extrinsic curvature and conformal factor have been solved on a dense lattice with 5000x200 points with the help of excellent numerical algorithms for sparse linear systems: MUMPS [13], UMFPACK [14] and HYPRE [15]. The precision was tested on the conformal factor of the Kerr solution (19), and for instance the mass parameter was recovered with the relative error less than 10^{-4} .

We have achieved still better precision using finite elements method (FEM). This method is based on triangulations which can be fitted to a shape of successive approximations of the solution. Especially powerfull has turned out to be the program FreeFem++ [8] which is an implementation of the special language dedicated to the finite element method. We have used it extensively as

it enables one to solve easily PDE problems, both elliptic and time dependent. The relative numerical precision has been improved up to 10^{-6} .

4.2 Detailed results

Our boundary conditions assume the slices to be asymptotically flat. The ADM mass is defined as

$$m_{ADM} = \sqrt{E^2 - P_i P_i}, \quad (45)$$

where E is the total energy of the system

$$E = -\frac{1}{2\pi} \int_{S_\infty} d^2 S^i \nabla_i \psi = \lim_{r \rightarrow \infty} 2r(\psi(r, \theta) - 1), \quad (46)$$

and P_i the total momentum defined in (41). The ADM mass is a parameter which shows how quickly a slice becomes flat at infinity. The minimal surface is in turn a closed surface which locally has a minimal area (in the riemannian geometry). The following inequality has been proved for slices with the vanishing extrinsic curvature [16], [17]

$$m_{ADM} \geq \sqrt{\frac{S}{16\pi}}. \quad (47)$$

Here m is the ADM mass and S the area of the outermost minimal surface. This is the so-called Riemannian version of the Penrose inequality [18], [19]. The minimal surface can be found from the condition

$$\nabla_i n^i = 0, \quad (48)$$

where n^i is the unit vector normal to the surface. The Penrose inequality must be reformulated for slices with non-vanishing extrinsic curvature. The minimal surface is then replaced by an apparent horizon by which is understood a closed two-dimensional surface which obeys one of the two equations [20]

$$\theta_\pm = \nabla_i n^i \mp K_{ij} n^i n^j = 0, \quad (49)$$

where \pm correspond to the past and future apparent horizons respectively, and θ_\pm are called optical scalars. In the axially symmetric case these apparent horizons satisfy the differential equations [1]

$$\begin{aligned} & r_{\theta\theta} + \frac{r_\theta^3}{r^2} \left(\frac{4\psi_\theta}{\psi} - \frac{q_\theta}{2} + \cot\theta \right) - r_\theta^2 \left(\frac{4\psi_r}{\psi} - \frac{q_r}{2} + \frac{3}{r} \right) \\ & + r_\theta \left(\frac{4\psi_\theta}{\psi} - \frac{q_\theta}{2} + \cot\theta \right) - r^2 \left(\frac{4\psi_r}{\psi} - \frac{q_r}{2} + \frac{2}{r} \right) = \\ & \pm \frac{1}{\psi^4} \sqrt{1 + \frac{r_\theta^2}{r^2}} (r^2 \hat{K}_{rr} + \frac{r_\theta^2}{r^2} \hat{K}_{\theta\theta} - 2r_\theta \hat{K}_{r\theta}), \end{aligned} \quad (50)$$

with the following boundary conditions for a function $r(\theta)$ at $\theta = 0$ and $\theta = \pi$

$$r_\theta|_{\theta=0} = r_\theta|_{\theta=\pi} = 0. \quad (51)$$

The Penrose conjecture for a slice with a non-vanishing extrinsic curvature has the same form (47) as before, but S is the area of the outermost apparent horizon to the future instead of the minimal surface. The above formulation is one of a number of possible wordings of the hypothesis - see [20] for an extensive discussion of various formulations of the Penrose conjecture. In fact all the versions described in [20] have been checked. Since the results differ very little and the hypotheses always stand the tests, we report here only data concerning the Penrose inequality described above. This inequality is not proved as yet although there are some partial results [12], [21], [22], [23], [24], [25] and schemes for the proof [26], [27]. It is widely believed that if the Penrose inequality is not true then the cosmic censorship will be broken.

Our numerical program was the following one

- for given values of Kerr parameters m, a solve the momentum constraints,
- calculate the conformal factor ψ for several values of the black hole momentum $P = \sqrt{P_i P^i}$ (41),
- for each P find the ADM mass, an apparent horizon and its area

$$S = 2\pi \int_0^a \psi^4 \exp\left(-\frac{q}{2}\right) \sqrt{r_\theta^2 + r^2} r \sin \theta d\theta,$$

- graphically show the momentum dependence of the coefficient

$$\epsilon_K = \sqrt{\frac{S}{16\pi m_{ADM}^2}},$$

which according to the Penrose inequality should satisfy the inequality $\epsilon_K \leq 1$.

The numerical results are presented on three figures (Fig. 1-3). Each of them shows how ϵ_K depends on momentum in case of Bowen-York and puncture boundary conditions.

Let us note that this dependence is quite different for the Bowen-York and the puncture boundary conditions. In the Bowen-York case the coefficient ϵ_K reaches some maximum, that is evident especially for big values of a .

There is also another inequality which is expected to hold for every axially symmetric, asymptotically flat initial data. Similarly to the Penrose inequality we can define a coefficient ϵ_A

$$\epsilon_A = \sqrt{\frac{S}{8\pi(m_{ADM}^2 + \sqrt{m_{ADM}^4 - J^2})}}, \quad (52)$$

where J is the total angular momentum. It is important to note that in our case

$$J = ma, \quad (53)$$

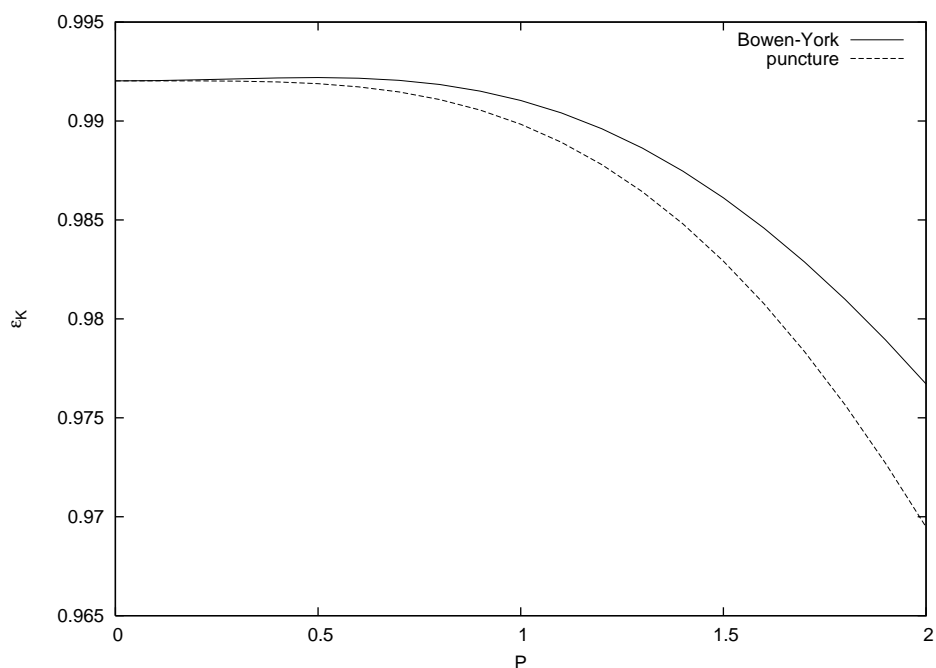


Figure 1: The momentum dependence of ϵ_K for $a = 0.5$ and $m = 2$.

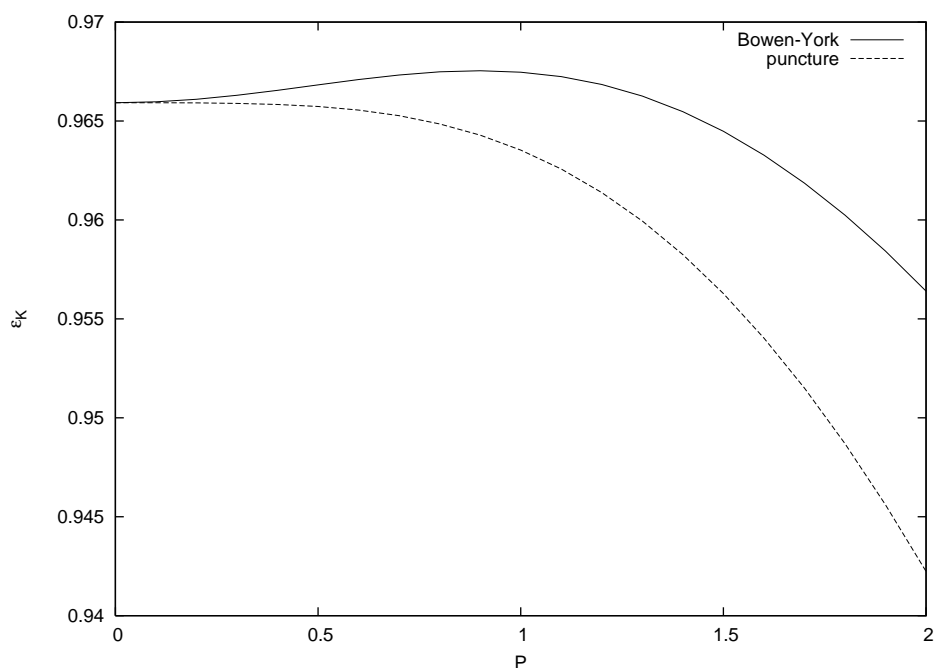


Figure 2: The momentum dependence of ϵ_K for $a = 1.0$ and $m = 2$.

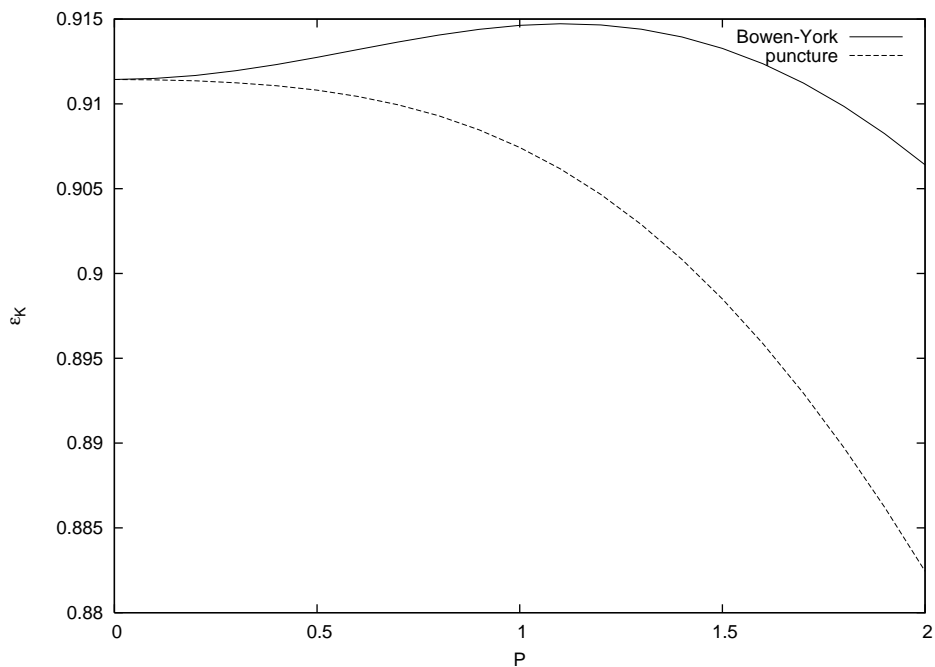


Figure 3: The momentum dependence of ϵ_K for $a = 1.5$ and $m = 2$.

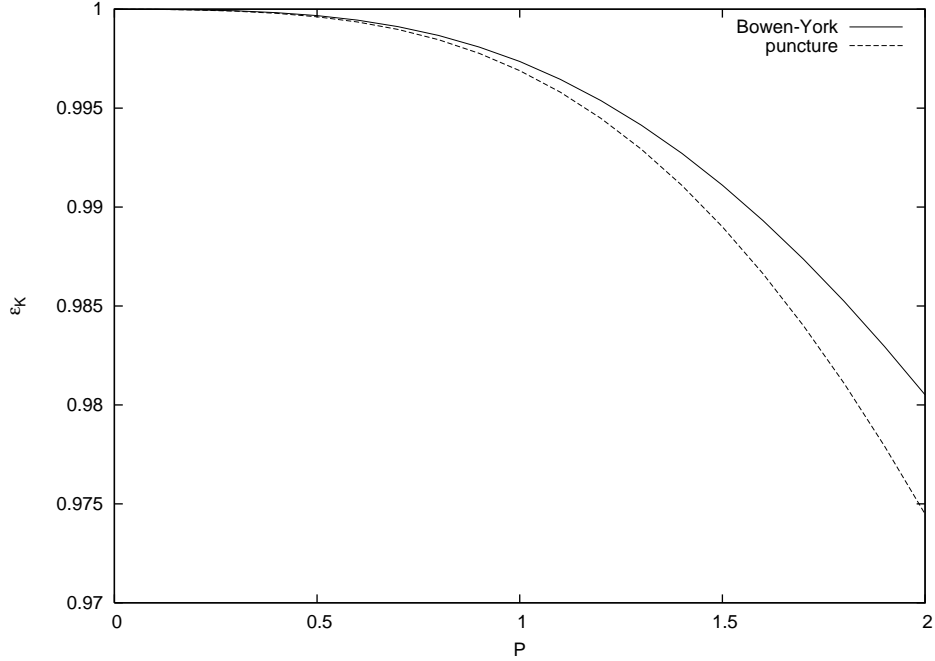


Figure 4: The momentum dependence of ϵ_A for $a = 0.5$ and $m = 2$.

even if the total momentum is not zero. The axially symmetric counterpart of the Penrose inequality can be stated as

$$\epsilon_A \leq 1,$$

and the equality is reached only for Kerr slices [28]. The momentum dependence of the coefficient ϵ_A both for Bowen-York and puncture data is shown on Fig. 4-6 .

Let us stress that our results depend only of two parameters $a = \frac{J}{m}$ and $\frac{P}{m}$. Therefore we have limited ourselves to $m = 2$.

5 Conclusions

We have generalized Bowen-York and puncture constructions of black hole initial data to the case of a boosted Kerr black hole in the axially symmetric case. These initial data smoothly depend on the black hole angular momentum and for $a = 0$ coincide with the conformally flat solutions. Our initial data are very precise and can serve as the starting point in constructing initial data for binary black holes. It would be also interesting to compute the long-term numerical evolution of the single boosted Kerr black hole and look for the quasinormal modes present in the radiation. We have calculated numerically the apparent

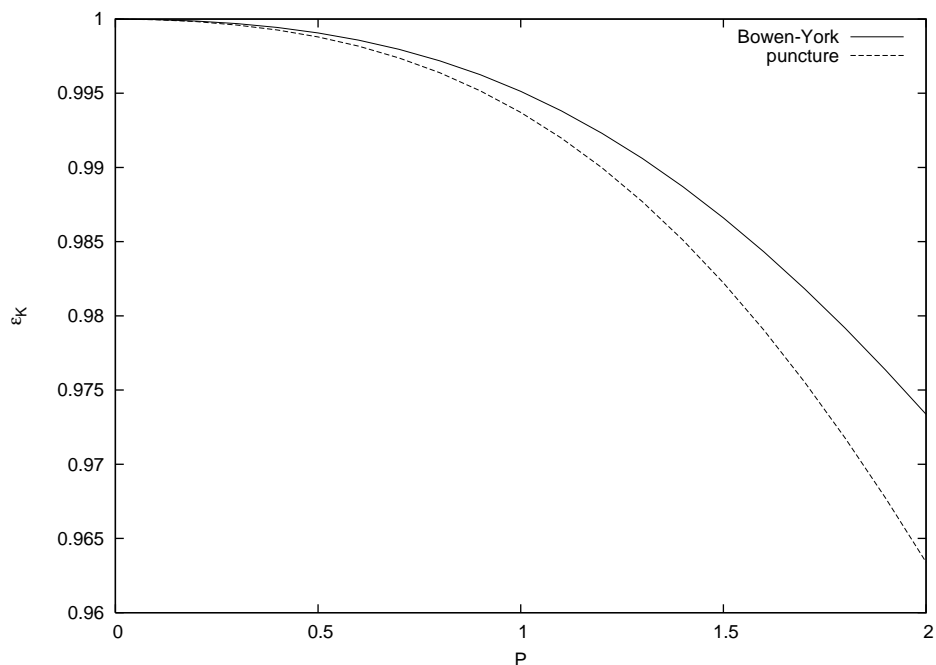


Figure 5: The momentum dependence of ϵ_A for $a = 1.0$ and $m = 2$.

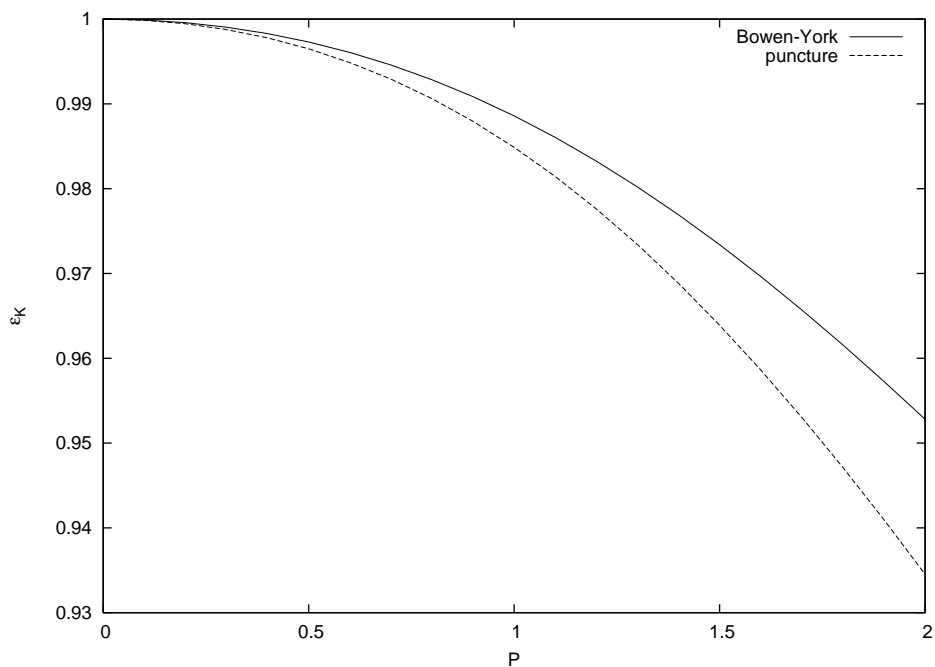


Figure 6: The momentum dependence of ϵ_A for $a = 1.5$ and $m = 2$.

horizons and tested the famous Penrose inequality together with its more restrictive version valid for axially symmetric initial data only. The numerical results are in agreement with theoretical predictions and clearly confirm the fact that the equality in the axially symmetric version is possible only for non-boosted Kerr black hole.

Our numerical calculations were mostly based on finite element method (FEM) techniques. In our opinion these methods lead to more precise results than those made on rectangular grids. The strength of FEM lies in the fact that the FEM algorithms have been widely tested in other areas of physics especially in elasticity, aerodynamics, electrostatics and in time dependent problems in hydrodynamics.

We believe that our results can be generalized in a straightforward manner to the case of binary black hole initial data. The work concerning appropriate puncture construction is in progress.

Acknowledgement. The author thanks prof. E. Malec for careful reading of the manuscript and helpfull comments and suggestions. This work was partly supported by the Polish State Committee for Scientific Research (KBN) grant 1 PO3B 01229.

References

- [1] J. M. Bowen and J. W. York, *Phys. Rev. D* **21** (1980) 2047.
- [2] S. Brandt and B. Brügmann, *Phys. Rev. Lett.* **78** (1997) 3606.
- [3] G. B. Cook, *Initial Data for Numerical Relativity*, *Living Rev. Rel.* **3** (2000) 5.
- [4] S. Dain, C. O. Lousto and R. Takahashi, *Phys. Rev. D* **65** (2002) 104038.
- [5] A. Garat, R. H. Price, *Phys. Rev. D* **61** (2000) 124011.
- [6] J. Karkowski and E. Malec, *On conformally flat initial data for Einstein equations*, gr-qc/0409032.
- [7] S. Dain and H. Friedrich, *Commun. Math. Phys.* **222**, 569 (2001).
- [8] <http://www.freefem.org/>, <http://www.dealii.org/>.
- [9] C. W. Misner, K. S. Thorne, J. A. Wheeler, *Gravitation*, W. H. Freeman and Company, New York, 1973.
- [10] D. Brill, *Ann. Phys.* **7** (1959) 466.
- [11] J. Karkowski, P. Koc and Z. Świerczyński, *Class. Quantum Grav.* **11** (1994) 1535.

- [12] J. Karkowski, E. Malec and Z. Świerczyński, *Class. Quantum Grav.* **10** (1993) 1361.
- [13] P. R. Amestoy, I. S. Duff and J.-Y. L'Excellent , Multifrontal parallel distributed symmetric and unsymmetric solvers, in *Comput. Methods in Appl. Mech. Eng.*, **184**, 501-520 (2000), <http://graal.ens-lyon.fr/MUMPS/>.
- [14] Algorithm 832: UMFPACK - an unsymmetric-pattern multifrontal method with a column pre-ordering strategy, T. A. Davis, *ACM Trans. Math. Software*, **vol 30**, no. 2, pp. 196-199, 2004, <http://www.cise.ufl.edu/research/sparse/umfpack/>.
- [15] R.D. Falgout and U.M. Yang, hypre: a Library of High Performance Preconditioners, in Computational Science - ICCS 2002 Part III, P.M.A. Sloot, C.J.K. Tan, J.J. Dongarra, and A.G. Hoekstra, eds., vol. 2331 of *Lecture Notes in Computer Science*, Springer-Verlag, 2002, pp. 632-641, <http://www.llnl.gov/CASC/hypre/>.
- [16] G. Huisken and T. Ilmanen, *J. Diff. Geom.*, **59** (2001) 353.
- [17] H. Bray, *J. Diff. Geom.*, **59** (2001) 177.
- [18] R. Penrose, *Ann. N. Y. Acad. Sci.* , **224**, 125 (1973).
- [19] G. Gibbons, p. 194 in Global Riemannian Geometry (T. J. Willmore and N. J. Hitchin, eds.), Ellis Harwood, Chichester 1984; *Class. Quantum Grav.*, **14**, 2509 (1997).
- [20] J. Karkowski and E. Malec, *Acta Phys. Pol. B36*, 59 (2005).
- [21] E. Malec and N. O'Murchadha, *Phys. Rev. D49*, 6931 (1994).
- [22] M. Iriondo, E. Malec and N. O'Murchadha, *Phys. Rev. D54*, 4792 (1996).
- [23] S. Hayward, *Phys. Rev. Lett.* **81**, 4557 (1998).
- [24] J. Jezierski, *Acta Phys. Pol. B25*, 1413 (1994).
- [25] J. Frauendiener, *Phys. Rev. Lett.* **87**, 101101-1(2001).
- [26] E. Malec, M. Mars and W. Simon, *Phys. Rev. Lett.* **88**, 1221102 (2002).
- [27] K. Roszkowski and E. Malec, *Acta Phys. Pol. B36*, 2931 (2005).
- [28] S. Hawking, *Comm. Math. Phys.* **25** (1972) 152.